2026 IEEE International Conference on Robotics and Automation (ICRA 2026)
June 1-5, 2026. Vienna, Austria

PRED-MPPI: Disturbance-Preview and Efficient MPPI for Robust Quadrotor Tracking with Hardware Validation

Haodi Zhang[1,*], Junwei Ge[1,*], Jinya Su[1], Yongping Pan[1], Jun Yang[2], *IEEE Fellow*, Wen-Hua Chen[3], *IEEE Fellow* and Shihua Li[1], *IEEE Fellow*

***Abstract*— We propose PRED-MPPI, the first MPPI variant that seamlessly integrates real-time disturbance preview and adaptive discretization for quadrotor tracking control under significant model inaccuracies and time-varying disturbances. Unlike prior MPPI variants (e.g., $\mathcal{L}_1$-MPPI, DA-MPPI), which assume constant or matched disturbances, PRED-MPPI leverages a high-order Generalized Extended State Observer for disturbance preview and a Variable Discretization Grid (VDG) to reduce computation and control variance. The synergy enables real-time (50 Hz) quadrotor control under time-varying and mismatched disturbances. Extensive comparative simulation and real-world Crazyflie experiments demonstrate substantial performance gains. In AirSim simulation, PRED-MPPI reduces computation time by over 30%, and mean RMSE by 10.3%, 13.5%, and 14.6% compared to baseline MPPI, and by 2.59%, 3.62%, and 5.80% compared to DA-MPPI across three representative scenarios. In real-world Crazyflie experiments, for ground-effect-disturbed hovering, PRED-MPPI reduces mean and standard deviation (Std) of X–Y plane error by 14.2%/17.9% and 6.03%/21.6% compared to MPPI and DA-MPPI; for fan-induced wind experiments, PRED-MPPI yields improvements of 23.4%/36.8% and 13.8%/25.0% in RMSE and tracking error Std. These results establish PRED-MPPI as the first disturbance-preview MPPI achieving real-world UAV robustness and efficiency, paving the way for deployment on resource-limited robotic platforms. GitHub page with videos is at `https://pred-mppi.github.io/`**

***Index Terms*— Disturbance-aware Control, Disturbance Preview, MPPI, Real-time Control, UAV Control**

I. INTRODUCTION

Model Predictive Path Integral (MPPI) control has become a powerful framework for robotics tasks such as path planning, locomotion, and trajectory tracking, owing to its ability to exploit GPU parallelism and flexibly incorporate diverse prediction models and cost functions [1], [2]. However, as a sampling-based variant of Model Predictive Control (MPC), its performance depends heavily on the accuracy of the surrogate model representing real dynamics. Unmodeled effects, parameter uncertainties, and external disturbances can degrade prediction fidelity and limit robustness in real-world disturbance-rich applications [3]. A motivating example is a small quadrotor flying close to the ground and under unknown wind. The UAV experiences *mismatched, time-varying disturbances* from both ground effect and unknown airflow, which cannot be handled by standard MPPI [1], $\mathcal{L}_1$-MPPI [4], or DA-MPPI [5].

Addressing such uncertainties has long been a focus of disturbance rejection control [6], [7]. Key challenges include unmodeled dynamics (e.g., UAV ground effect), unmeasurable parameters (e.g., aerodynamic coefficients), and unknown external disturbances (e.g., wind) [8]. While refined modeling and learning-based identification have advanced [9], [10], these approaches are generally computationally intensive, limiting their real-time applications. Alternatively, lumped disturbances can be estimated online and utilized accordingly, as in Disturbance Observer (DOB)-based MPC [11], [12] and $\mathcal{L}_1$-adaptive MPC [4].

However, most state-of-the-art (SOTA) DOB-augmented strategies are tailored to explicit optimization-based MPC frameworks rather than sampling-based methods such as MPPI in this study, preventing them from fully exploiting GPU acceleration and flexible costs [2]. In addition, many employ simple feedforward disturbance compensation under the strong assumption that mismatched disturbances can be inherently suppressed by low-level controllers [4]-an assumption that often fails in disturbance-rich environments. In practice, disturbances are frequently both time-varying and mismatched, making their rejection within the MPPI framework a non-trivial challenge and a critical open research gap.

Building on the SOTA DA-MPPI framework [5], we propose PRED-MPPI, the first MPPI variant to integrate real-time disturbance preview via a Generalized Extended State Observer (GESO) [13] into the trajectory sampling process. In parallel, a Variable Discretization Grid (VDG) strategy [14] allocates finer temporal resolution early in the horizon and coarser resolution later, reducing computation time and control input variance without compromising accuracy. This combination enables effective rejection of time-varying, mismatched disturbances while further improving MPPI's computational efficiency.

The framework is validated in both high-fidelity AirSim simulations and real-world Crazyflie quadrotor experiments.

*Contribute equally. This work was supported by the National Natural Science Foundation of China under Grant 62303110, Start-Up Research Fund of Southeast University under Grant RF1028623226, Nanjing Major Science and Technology Special Project under grant number 202309017, and Xiaomi Young Talents Program. Corresponding author: Prof. Jinya Su.

[1]Haodi Zhang, Junwei Ge, Jinya Su, Yongping Pan and Shihua Li are with School of Automation, Key Laboratory of Measurement and Control of CSE, Ministry of Education, and Institute of Intelligent Unmanned Systems, Southeast University, Nanjing 210096, China. `220232102@seu.edu.cn; 220242214@seu.edu.cn; sucas@seu.edu.cn; panyp@seu.edu.cn; lsh@seu.edu.cn`

[2]Jun Yang is with the Department of Aeronautical and Automotive Engineering, Loughborough University, LE11 3TU, United Kingdom. `J.Yang3@lboro.ac.uk`

[3]Wen-Hua Chen is with the Research Centre for Low Altitude Economy and the Department of Aeronautical and Aviation Engineering, The Hong Kong Polytechnic University, Hong Kong, China. `wenhua.chen@polyu.edu.hk`

To the best of our knowledge, PRED-MPPI is the *first* MPPI variant that simultaneously integrates disturbance preview and adaptive discretization, and demonstrates their synergy on real UAV hardware, the detailed contributions are summarized in threefold:

(1) **PRED-MPPI framework**: First integration of disturbance preview into MPPI, enabling robust control under time-varying and mismatched disturbances.
(2) **Adaptive discretization**: Incorporation of VDG into MPPI trajectory rollouts to reduce computation and control variance while maintaining accuracy.
(3) **Comparative validation**: Extensive comparative simulation and real-world Crazyflie experiments show superior tracking accuracy and robustness over baseline geometric PD controller, MPPI, DA-MPPI and their VDG-enhanced variants.

Together, these advances position PRED-MPPI as a practical, high-performance control framework for real-time, disturbance-rich robotic applications, bridging robust disturbance rejection with the computational efficiency needed for deployment on resource-constrained platforms.

II. Related Work

A. MPPI in Robotics

Advances in parallel computing, particularly GPU acceleration via CUDA, have facilitated the adoption of variational inference-based MPC methods such as MPPI and the Cross-Entropy Method in diverse robotic domains, including autonomous driving [15], bipedal locomotion [16], and robotic manipulation [17]. These methods offer high flexibility in system modeling, cost design, and optimization while maintaining computational efficiency. The seminal MPPI work [18] demonstrated significant speedups in multi-agent navigation (9 quadrotors, 144 states), proving its scalability for high-dimensional problems.

Since then, MPPI variants have been developed to overcome practical challenges. For example, [19] achieves aggressive off-road driving by embedding a detailed first-principles model with residual dynamics. [20] employs a learning-based generalist dynamics model for MPPI, enabling agile control across heterogeneous wheeled robots. Other work (e.g., diffusion-MPPI [21]) improves robustness and precision by adapting the sampling distribution within rollout dynamics [22]. While these studies showcase MPPI's adaptability, they generally focus on model fidelity and sampling efficiency, with less emphasis on disturbance rejection in sampling-based MPC.

B. Disturbance-Aware Predictive Control

Robust predictive control methods often incorporate disturbance compensation to improve tracking accuracy and resilience, ranging from simple feedforward schemes to disturbance-augmented prediction models and preview-based approaches [6]. For instance, [23] uses feedforward wind disturbance compensation in explicit MPC for small helicopters. [11] augments the prediction model with constant disturbance estimates, while [12] incorporates disturbance preview to improve offset-free MPC under time-varying conditions.

By contrast, disturbance-aware MPPI has seen limited exploration. Existing approaches, such as [24], [25], adopt conservative robust control strategies with single-degree-of-freedom paradigms. Active disturbance rejection in MPPI remains rare. Notably, [4] proposes an $\mathcal{L}_1$-adaptive MPPI for agile quadrotor flight, but it relies on feedforward compensation and assumes mismatched disturbances can be suppressed by low-level controllers-an assumption that frequently breaks down in disturbance-rich environments.

TABLE I: Comparisons of representative MPPI algorithms. **Bold blue** indicates our proposed method.

Methods	Mismatched	Dis Type	Grid	Experiment
MPPI	–	–	Constant	✓
$\mathcal{L}_1$ MPPI	×	Constant	Constant	✓
DA-MPPI	✓	Constant	Constant	×
PRED-MPPI	✓	**Generic**	**Variable**	✓

Open Gap (before our work): *No MPPI handles time-varying, mismatched disturbances with variable grids and hardware validation.*

Mismatched: supporting mismatched disturbance or not; *Dis Type*: constant or generic disturbance; *Grid*: constant or variable discretization grids in the prediction horizon.

Table I summarizes representative MPPI variants, comparing their disturbance entry type (supporting mismatched or not), disturbance type, discretization strategy, and experimental validation. As shown, existing methods handle either matched disturbances or constant disturbance, and none combine generic disturbance with variable discretization grids in a framework validated with hardware experiment. This gap motivates the proposed PRED-MPPI, which integrates generic disturbance preview and variable-grid rollouts, and validates them in simulation and real-world experiments.

C. Model-Based Quadrotor Control

Quadrotor control has inspired various model-based strategies to mitigate modeling inaccuracies [26]. [27] introduced a geometric controller on the $SE(3)$ manifold for globally stable trajectory tracking. [8] enhances nonlinear MPC with residual dynamics for improved landing performance. Recent efforts balance computational efficiency and safety, such as combining variational inference MPC with reachability analysis [28]. Our work advances this line by extending the DA-MPPI framework with a high-order GESO for disturbance preview and a VDG for computational efficiency. This integration with experimental validation enables PRED-MPPI to address time-varying, mismatched disturbances while reducing computational load and control variance, a capability not present in prior MPPI quadrotor controllers.

III. Modeling and Problem Formulation

We consider a simplified quadrotor UAV modeled as a rigid body with four identical rotors mounted at the ends of orthogonal arms. The rotors generate thrust force (f) and angular velocity ($\boldsymbol{\Omega}_{1:3}$) in body frame, collectively represented as the control input $\boldsymbol{u}$, as seen in Fig. 1. The

UAV motion evolves on the special Euclidean group $SE(3)$, where translation describes the center of mass trajectory in the inertial frame and rotation describes the attitude of the body-fixed frame relative to the inertial frame. We denote the inertial frame by $\{\boldsymbol{e}_1, \boldsymbol{e}_2, \boldsymbol{e}_3\}$ and the body-fixed frame by $\{\boldsymbol{b}_1, \boldsymbol{b}_2, \boldsymbol{b}_3\}$, both defined as right-handed coordinate systems. The total thrust vector is aligned with $\boldsymbol{b}_3$. The nominal dynamics of the quadrotor can be expressed as,

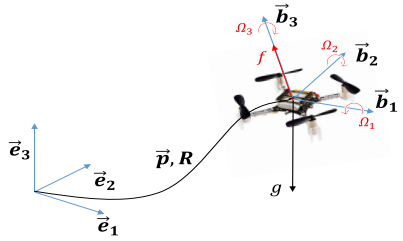

Fig. 1: Coordinate and dynamics of the Crazyflie Quadrotor

$$\begin{cases} \dot{\boldsymbol{p}} = \boldsymbol{v}, \\ m\dot{\boldsymbol{v}} = f\boldsymbol{R}\boldsymbol{e_3} - mg\boldsymbol{e_3}, \\ \dot{\boldsymbol{R}} = \boldsymbol{R}\hat{\boldsymbol{\Omega}}, \end{cases} \tag{1}$$

where $\boldsymbol{p}$, $\boldsymbol{v}$, R, and $\boldsymbol{\Omega}$ denote quadrotor position, velocity, orientation, and angular velocity. m is the vehicle mass, and $\hat{\boldsymbol{\Omega}}$ is the skew-symmetric matrix of $\boldsymbol{\Omega}$. In practice, the control input $\boldsymbol{u}$ is mapped to the target angular velocity commands $\boldsymbol{u}_{1:4}$ for the low-level rotor speed controller. Following the Crazyflie platform[1], we define the control vector as $\boldsymbol{u} = [f, \Omega_1, \Omega_2, \Omega_3]^T$, where $\Omega_1, \Omega_2, \Omega_3$ represent roll, pitch, and yaw angular velocities in body frame.

In real-world operation, aggregate disturbances, arising from unmodeled aerodynamics, internal parameter uncertainties, or external perturbations such as wind, inevitably introduce discrepancies between the nominal model and actual quadrotor dynamics, as depicted in Eq. (2) with the lumped disturbance $\boldsymbol{d}(t)$ in position channel. For instance, deviations in the estimated mass m or tracking errors from the low-level motor controller can significantly affect the performance of the attitude loop. In such cases, relying solely on feedforward disturbance compensation in the position controller is insufficient, since the applied correction in the acceleration channel is aligned with $\boldsymbol{b}_3$ and cannot fully capture inertia-induced discrepancies. Moreover, many model-based predictive controllers assume that disturbances remain constant over the prediction horizon, which leads to accumulated prediction errors and weakens disturbance rejection capability.

$$\begin{cases} \dot{\boldsymbol{p}} = \boldsymbol{v}, \\ \dot{\boldsymbol{v}} = \underbrace{\frac{f}{m}\boldsymbol{R}\boldsymbol{e_3} - g\boldsymbol{e_3}}_{\boldsymbol{h(R,u)}} + \boldsymbol{d}(t), \\ \dot{\boldsymbol{R}} = \boldsymbol{R}\hat{\boldsymbol{\Omega}} \end{cases} \tag{2}$$

[1]As noted in the Crazyflie community and confirmed in our experiments, directly commanding motor PWM signals leads to instability due to the limited bandwidth, delay, and packet drop rate of wireless links. Hence, we employ thrust and body-frame angular velocities (cmdvel) as control inputs.

The problem under consideration is to track a reference trajectory using MPPI with the simplified quadrotor nominal model under complex and time-varying disturbances $\boldsymbol{d}(t)$ while satisfying state and input constraints.

IV. Methodology

A. Disturbance Preview

In Section III, we analyzed quadrotor dynamics under aggregated disturbances, as formulated in Eq. (2). Prior work such as [4] incorporates disturbance compensation into MPPI via a feedforward scheme, but relies on the fragile assumption that mismatched disturbances can be indirectly mitigated by the low-level attitude controller. DA-MPPI [5] advances this by embedding disturbance estimates directly into the MPPI prediction model; however, it assumes disturbances remain constant over the prediction horizon. While this simplification may hold under slow or near-stationary disturbances ($\dot{\boldsymbol{d}} \approx 0$), predictive fidelity degrades significantly under time-varying disturbances.

To effectively address time-varying disturbances, we incorporate a disturbance preview mechanism into MPPI by exploiting disturbance derivative information and applying Taylor expansion within the receding horizon. This enables more accurate disturbance modeling and preview (prediction), thereby enhancing robustness against time-varying, mismatched disturbances. The disturbance preview in the prediction horizon is given as below.

$$\boldsymbol{d}(t+\tau) = \boldsymbol{d}(t) + \dot{\boldsymbol{d}}(t) \cdot \tau + \boldsymbol{R_2}(t)$$

where $\boldsymbol{d}(t)$ and $\dot{\boldsymbol{d}}(t)$ denote disturbance and disturbance derivative at t, and higher-order disturbance terms are omitted and denoted as $\boldsymbol{R_2}(t)$. Estimating $\boldsymbol{d}(t)$ and $\dot{\boldsymbol{d}}(t)$ via observer technique is presented below.

For generality, and given that positional dynamics are most affected by the first two terms in Eq. (2), we adopt a high-order GESO [29], formulated in Eq. (3). This observer provides disturbance and disturbance derivative estimation with guaranteed convergence (see, [29] for proof), while maintaining robustness to noise in partially measured states.

$$\begin{cases} \dot{\hat{\boldsymbol{p}}} = \hat{\boldsymbol{v}} + L_1 \cdot (\boldsymbol{p} - \hat{\boldsymbol{p}}), \\ \dot{\hat{\boldsymbol{v}}} = \boldsymbol{h(R,u)} + \hat{\boldsymbol{d}}_{\boldsymbol{1}} + L_2 \cdot (\boldsymbol{p} - \hat{\boldsymbol{p}}), \\ \dot{\hat{\boldsymbol{d}}}_{\boldsymbol{1}} = \hat{\boldsymbol{d}}_{\boldsymbol{2}} + L_3 \cdot (\boldsymbol{p} - \hat{\boldsymbol{p}}), \\ \dot{\hat{\boldsymbol{d}}}_{\boldsymbol{2}} = L_4 \cdot (\boldsymbol{p} - \hat{\boldsymbol{p}}) \end{cases} \tag{3}$$

where L_i $(i = 1, 2, 3, 4)$ are observer gains based on pole placement or bandwidth approach, $\hat{\boldsymbol{p}}, \hat{\boldsymbol{v}}$, $\hat{\boldsymbol{d}}_{\boldsymbol{1}}$ and $\hat{\boldsymbol{d}}_{\boldsymbol{2}}$ are estimated position, velocity, lumped disturbance and its derivative, $\boldsymbol{p}$ is the measurement of position.

Once the disturbance and its derivative have been estimated as $\hat{\boldsymbol{d}}_{\boldsymbol{1}}, \hat{\boldsymbol{d}}_{\boldsymbol{2}}$, the disturbance preview module can be conveniently formulated as $\hat{\boldsymbol{d}}(t+\tau) = \hat{\boldsymbol{d}}_{\boldsymbol{1}} + \hat{\boldsymbol{d}}_{\boldsymbol{2}} \cdot \tau$ within the MPPI rolling dynamics in Eq. (2).

Remark 1. *In real-time applications, GESO's order in (3) can be further adjusted to balance estimation accuracy and*

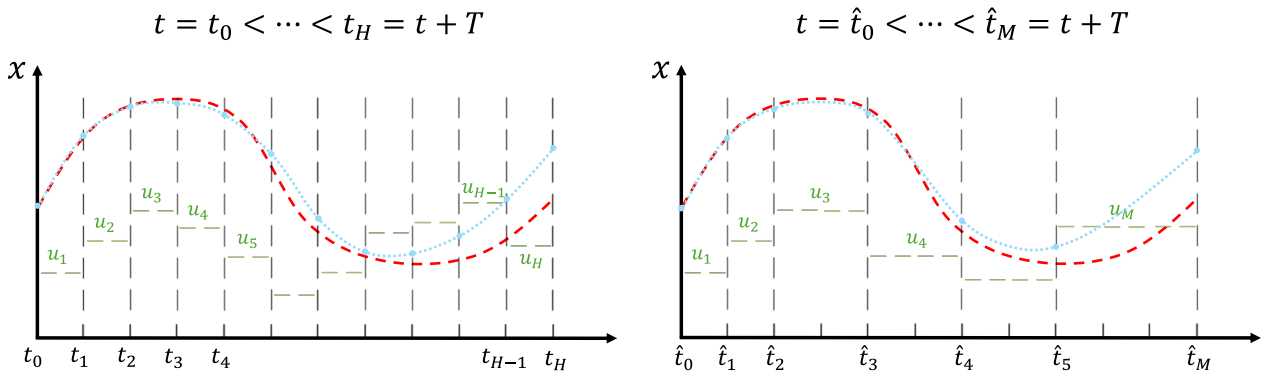

(a) Standard Uniform Discretization Grids

(b) Input Variable Discretization Grids

Fig. 2: Comparison between uniform and variable discretization grids: VDG allocates finer steps early (higher sensitivity) and coarser steps later (lower sensitivity), reducing variance while maintaining accuracy.

computational efficiency [29]. Note that excessively high-order estimators may impose additional estimation burdens, thereby degrading convergence performance.

B. Variable Discretization Grids

Standard multiple shooting predictive control methods adopt a uniformly discretized grid in prediction horizon to formulate the optimal control framework. Nevertheless, the standard uniform grid partition lacks the consideration of the increasing model discrepancy within prediction horizon, wasting precious computation resources in the inaccurate bracket namely $[t_4, \ldots, t_H]$ in Fig. 2a. Accordingly, it is intuitive to obtain that future disturbance information has a diminishing influence on the current control input [12].

Therefore, we utilize a variable discretization grid (VDG) depicted in Fig. 2b for better computational efficiency. Noting the total number of time steps in VDG formulation as M, it follows that $\sum_{i=1}^{H} \triangle t_i = \sum_{j=1}^{M} \triangle \hat{t}_j = T$, where H is the original number of time steps and T denotes the prediction horizon. Reducing the number of time steps not only significantly decreases the computation time but also reduces the variance of the weighted sum of control inputs, as demonstrated in [30]. Statistical ablation studies, as presented in Sec. V-B, further validate the effectiveness of the proposed VDG approach in reducing both computation time and the variance of tracking error.

Remark 2. ***Complexity Analysis:*** *Baseline MPPI requires $\mathcal{O}(N \cdot H)$ rollouts, where N is the number of sampled trajectories and H the uniform horizon length. PRED-MPPI reduces this to $\mathcal{O}(N \cdot M)$ with $M < H$ by adaptive discretization, achieving significant computational savings without loss of fidelity.*

C. PRED-MPPI Framework

Building on the disturbance preview mechanism in Section IV-A and the VDG strategy in Section IV-B, we propose the PRED-MPPI framework. As illustrated in Fig. 3, PRED-MPPI integrates the GESO for disturbance preview and the VDG strategy for computational efficiency. Together, these components enable accurate compensation of time-varying, mismatched disturbances while maintaining tractable online computation. MPPI employs importance sampling to generate an optimal control sequence. Within this context, consider the deterministic finite-horizon optimal control problem,

$$\begin{aligned} \min_{u_{1:M}} J(u_{1:M}) &= \sum_{i=1}^{M-1} c_h(x_i, u_i) + c_f(x_M) \\ s.t. \quad x_{i+1} &= f(x_i, u_i) \\ c_i(x_i, u_i) &< 0 \end{aligned} \tag{4}$$

where M is the number of VDG adjusted time steps, $c_h : \mathbb{R}^n \times \mathbb{R}^m \to \mathbb{R}_{\geq 0}$ and $c_f : \mathbb{R}^n \to \mathbb{R}_{\geq 0}$ denote running cost and terminal cost.

Note that within the context of sampling-based MPC, the hard constraints in the optimization problem (4) are typically relaxed into soft constraints by embedding them into the cost function. $f : \mathbb{R}^n \times \mathbb{R}^m \to \mathbb{R}^n$ characterizes the dynamics (e.g., Eq. (1) or (2)), and $c_i : \mathbb{R}^n \times \mathbb{R}^m \to \mathbb{R}_q$ represent states/input constraints. At every time step, the classical MPC solves Eq. (4) in a receding-horizon manner through optimization. However, its performance, which depends on certain formulations like sequential quadratic programming, deteriorates when Eq. (4) is highly non-convex due to the nonlinearity of dynamics f or non-convex c_h, c_f and c_i.

In the PRED-MPPI framework, sensor-based position measurements are first processed by the GESO, generating state estimates $\hat{\boldsymbol{p}}$ (position), $\hat{\boldsymbol{v}}$ (velocity), disturbance and its derivative estimates $\hat{\boldsymbol{d}}$, $\hat{\dot{\boldsymbol{d}}}$. These estimates are subsequently fed into the disturbance-aware rolling dynamics (2) in MPPI to compute the optimal control inputs f and $\boldsymbol{\Omega}$, which are subsequently transmitted to the low-level controller on the Crazyflie platform to convert the control inputs into the angular velocities of the four rotors. To ensure smooth control performance, the MPPI framework is formulated by sampling the derivative of the control input,

$$\boldsymbol{u}_k = \boldsymbol{u}_{k-1} + \Delta \boldsymbol{u}_k, \quad \Delta \boldsymbol{u}_k^i \sim \boldsymbol{N}(0, \boldsymbol{\Sigma}), \tag{5}$$

$$\Delta \boldsymbol{u}_k = \frac{\sum_{i=1}^{N} \Delta \boldsymbol{u}_k^i \cdot exp(-\frac{J(\boldsymbol{u}_k^i) - \beta}{\lambda})}{\sum_{i=1}^{N} exp(-\frac{J(\boldsymbol{u}_k^i) - \beta}{\lambda})}. \tag{6}$$

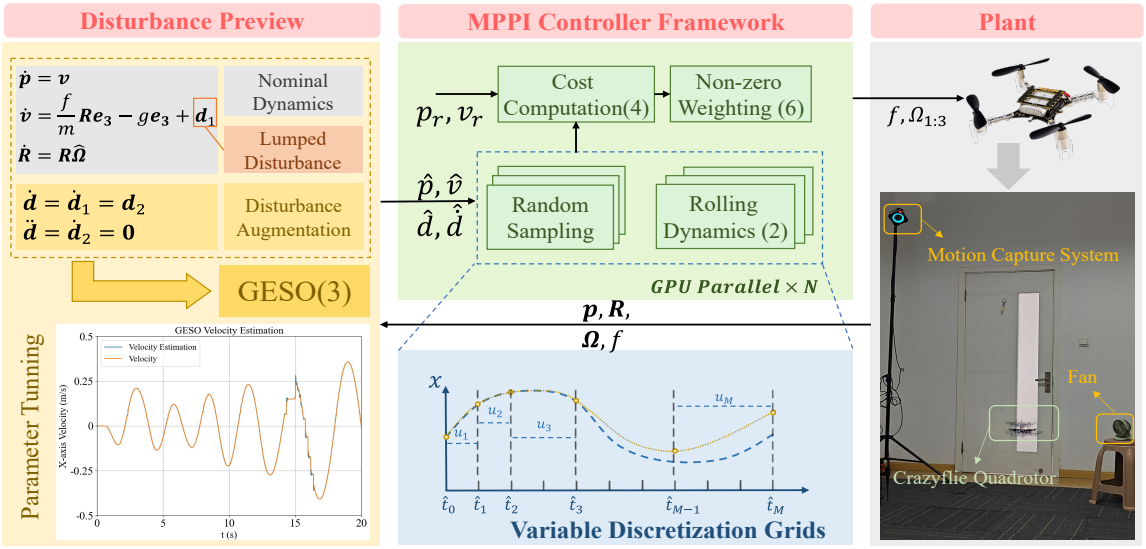

Fig. 3: PRED-MPPI integrating disturbance preview into MPPI rolling dynamics with variable discretization grids.

We utilize the numerically nonzero importance sampling weight in Eq. (6) to achieve numerical stability, where β is the minimum cost among N rollout trajectories, and $\lambda > 0$ is the temperature weight commonly used in stochastic control. A smaller λ could induce more centralized output, e.g., $\Delta \boldsymbol{u}_k = argmin(J(\boldsymbol{u}_k^i))$ as $\lambda \to 0$.

V. Comparative Validation

In this section, both simulations and experiments are conducted through Crazyflie trajectory tracking to validate the algorithm and answer the following questions:

- $\boldsymbol{Q_1}$ Can the VDG strategy enhance computational efficiency of the MPPI optimization process while maintaining algorithmic performance?
- $\boldsymbol{Q_2}$ To what extent can PRED-MPPI outperform the MPPI and DA-MPPI under complex disturbances despite simplification in model-based trajectory sampling?

A. Experimental Setup

We evaluate the proposed controllers in both simulation and real-world experiments. In simulation, experiments are conducted in the AirSim environment using the same parameter settings as [5]. The control architecture is implemented in PyTorch on a laptop equipped with an NVIDIA RTX 3060 GPU, running at a control frequency of 50 Hz, while the GESO module operates at 200 Hz. We evaluate performance on three representative trajectory primitives, zig-zag, lemniscate, and square, subjected to ramp-type disturbances that emulate time-varying external perturbations.

In hardware experiments, ground-truth states and position observations are obtained through Virtual-Reality Peripheral Network communication with a four-camera motion capture system (ChingMu MC1300). Exogenous wind disturbances are introduced using a miniature fan, as shown in Fig. 3. We consider two scenarios for concept validation: trajectory tracking in the presence of ground effect and circular trajectory tracking under fan-induced unknown time-varying wind disturbances.

Following [5], the prediction horizon is set to $H = 10$, representing the marginal threshold for stable quadrotor control in this setup. The number of sampled trajectories is fine-tuned to $N = 600$, ensuring compatibility with the 50 Hz control rate for the baseline MPPI controller. For the VDG strategy, the discretization grid is configured as $[1, 1, 1, 2, 2, 3]$, whose sum matches the horizon length $H = 10$, thereby achieving finer resolution in the near term and coarser resolution in later steps.

B. Simulation evaluation

To answer $\boldsymbol{Q1}$, we execute each designed trajectory for 20 times, where the statistical results in terms of computation time and control performance are shown in Figs 4, 5 visually and Table II quantitatively.

(1) Fig. 4 shows that MPPI leveraging VDG reduces computation time by over 30% thanks to the reduction in the number of sampled control inputs (or equivalently number of decision variables in classical MPC [14]).

(2) Box plot 5 and Table II indicate that integrating VDG in MPPI could reduce the variance of tracking error by 31.1%, 56.8% and 47.5% in three scenarios. This improvement stems from the reduced stochastic noise due to fewer sampled inputs, consistent with the analysis in [30].

To answer $\boldsymbol{Q2}$, we compare the trajectory tracking performance of MPPI baseline, MPPI+VDG, DA-MPPI+VDG and the proposed PRED-MPPI in three representative scenarios. The controllers' loss function is formulated as,

$$\min_{u_{1:H}} J(\boldsymbol{x}, \boldsymbol{v}, \boldsymbol{\theta}, \boldsymbol{\phi}, \boldsymbol{\psi}) = \sum_{i=1}^{H} (q_x \cdot \boldsymbol{e_x^T e_x} + q_v \cdot \boldsymbol{e_v^T e_v} + q_\psi \cdot \boldsymbol{\psi^T \psi} + f^2 + q_\Omega \cdot \Omega^T \Omega + q_c \cdot c(\theta, \phi, u)) \tag{7}$$

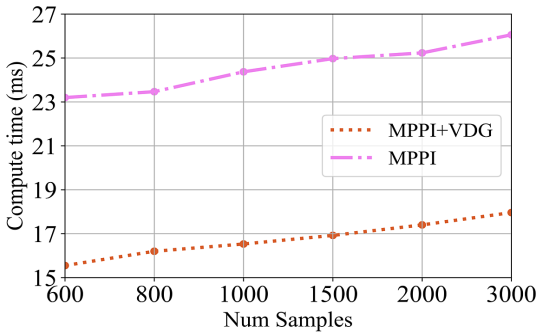

Fig. 4: Average computation time with varying numbers of sampled trajectories for MPPI with and without *VDG* strategy.

where θ, ϕ, ψ are quadrotor pitch, roll and yaw angle in body frame, $c(\theta, \phi, u) = clamp(\theta, \frac{\pi}{6}) + clamp(\phi, \frac{\pi}{6}) + clamp(f, (0, 0.5886))$ is soft constraint limiting pitch and roll angle within $\frac{\pi}{6}$, and thrust f within 0 to 0.5886N. The parameters are set to $q_x = 520, q_v = 30, q_\psi = 50, q_\Omega = 0.3$ and $q_c = 600$. The following observations can be drawn.

(1) As in Fig. 5, the proposed PRED-MPPI demonstrates superior performance against the classical MPPI, MPPI+VDG and DA-MPPI+VDG with reduced mean RMSE, particularly in the Lemniscate tracking experiment due to its smooth and tractable trajectory.
(2) Quantitative analysis in Table II further supports these findings, indicating that the PRED-MPPI reduces mean tracking error in terms of RMSE by 10.3%, 13.5% and 14.6% across three representative scenarios over the MPPI baseline. These results imply the advantages of incorporating disturbance preview and VDG into MPPI rolling dynamics.
(3) Compared to DA-MPPI+VDG, the proposed PRED-MPPI enhances the performance by 2.59%, 3.62% and 5.8% in terms of mean tracking error, which verifies the effectiveness of *disturbance preview*.

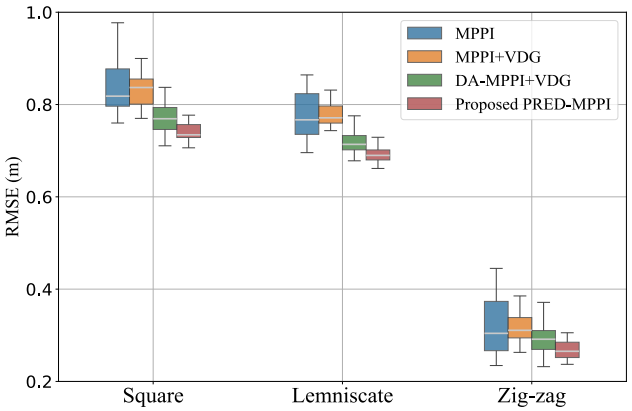

Fig. 5: Box plots of RMSE for three typical scenarios. The center line indicates the median, the box height represents the interquartile range (IQR).

TABLE II: Tracking error statistics in ground effect experiments (lower is better). Best in **blue bold**, second-best in gray.

Scenario	Metric	MPPI	MPPI+VDG	DA-MPPI+VDG	PRED-MPPI
Square	Mean	0.839	0.831	0.773	**0.753**
	Std	0.061	0.051	0.044	**0.038**
Lemniscate	Mean	0.801	0.780	0.719	**0.693**
	Std	0.095	0.041	**0.039**	0.042
Zig-zag	Mean	0.323	0.319	0.293	**0.276**
	Std	0.080	0.042	0.043	**0.037**

C. Real-World Crazyflie Experiments

1) Ground Effect Experiments: In this experiment, the altitude reference is set to $p_z = 0.5$ m to induce a pronounced nonlinear ground effect. Moreover, the quadratic relationship between thrust force (f) and PWM command (0–65535) is approximated as linear within the controllers, introducing additional input uncertainty. The cost functions of MPPI framework are the same as Eq. (7), with the parameters set to $q_x = 70, q_v = 15, q_\psi = 12, q_\Omega = 0.3$ and $q_c = 600$. For comparison, we evaluate six representative algorithms including the geometric $SE(3)$ PD controller [27], baseline MPPI [1] (with/without VDG strategy), DA-MPPI [5] (with/without VDG strategy), and the proposed PRED-MPPI.

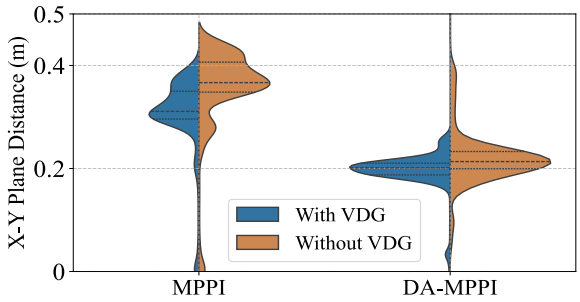

Fig. 6: Violin plots represent the distance to (0,0) in X-Y plane of the baseline controllers W/WO VDG strategy. The center dash line indicates the median, the dash dot line represents the IQR, and the colored zone is the distribution.

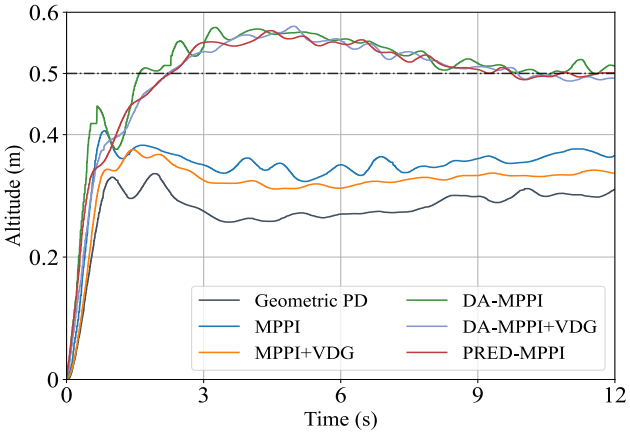

Fig. 7: Crazyflie altitude response under six control schemes, where dash dotted line at 0.5m denotes the target hovering height.

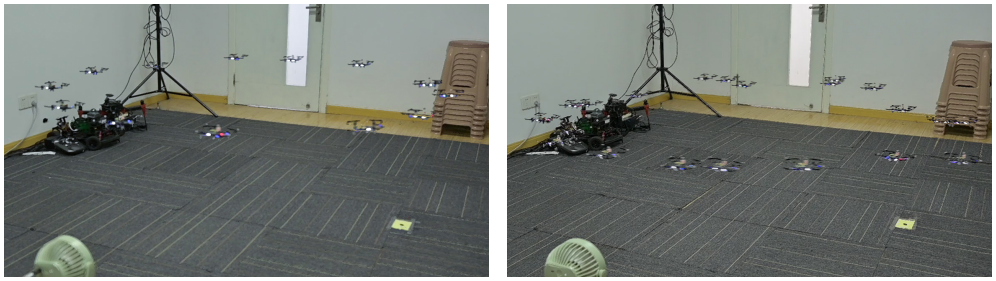

(a) PRED-MPPI experiments results (b) Baseline MPPI experiments results

Fig. 8: Comparison between baseline MPPI and the proposed PRED-MPPI under fan-induced wind disturbance.

(1) As in Fig. 6, integrating VDG with baseline controllers suppresses output noise, reducing both the mean and variance of the X–Y displacement distribution. Specifically, for MPPI, the mean/variance decrease from 0.352/0.089 to 0.302/0.073, while for DA-MPPI they reduce from 0.232/0.088 to 0.218/0.069. These results provide a concrete answer to $\boldsymbol{Q1}$.

(2) Fig. 7 shows that disturbance-unaware controllers (e.g., geometric PD, MPPI, and MPPI+VDG) fail to maintain the target altitude at $p_z = 0.5m$ due to ground effect and input uncertainties, whereas the disturbance-aware controllers (e.g., DA-MPPI, DA-MPPI+VDG, PRED-MPPI) successfully achieve the target. In particular, the proposed PRED-MPPI obtains the best results in terms of smoothness and tracking error.

A detailed comparison of their disturbance-rejection capabilities is presented in the subsequent trajectory-tracking under fan-induced unknown wind to better answer $\boldsymbol{Q2}$.

2) Fan-induced Wind Experiments: In this experiment, as shown in Fig. 8, the trajectory reference is set as a circle $p_x^2 + (p_y - 1)^2 = 1^2, p_z = 0.6m$ with linear velocity $v_r = 1m/s$ in X-Y plane. Moreover, the exogenous wind disturbance is generated by a tiny fan as in Fig. 3, with maximum wind speed of 2.8m/s in our experiments. Simultaneously, the Crazyflie quadrotor experiences nonlinear gust disturbances as it approaches the wall (illustrated in Fig.8 and the $y > 1.5m$ zone in Fig. 10), with input mapping uncertainty and candidate controllers as described in Section V-C.1. These combined highly nonlinear disturbances introduce substantial uncertainty. The comparative results are shown in Figs. 9, 10 and Table III. The following observations can be drawn.

TABLE III: Tracking error statistics in circular trajectory under wind (lower is better). Best in **blue bold**, second-best in gray.

Scenario	Metric	PD	MPPI	DA-MPPI	PRED-MPPI
Without VDG	RMSE	0.167	0.153	**0.137**	–
	Std	0.144	0.149	**0.096**	–
With VDG	RMSE	–	0.154	0.131	**0.118**
	Std	–	0.114	0.081	**0.072**

(1) It follows from Figs. 9, 10 that the proposed PRED-MPPI consistently outperforms the baseline controllers. Compared to the DA-MPPI controller, PRED-MPPI effectively predicts wind speed variations induced by the changing distance to the fan, thereby enhancing disturbance rejection capability.

(2) Table III shows that the PRED-MPPI achieves 9.92% and 13.8% reductions in RMSE over DA-MPPI W/WO VDG, while also reducing the tracking error standard deviation by 11.1% and 25.0%.

(3) Compared to the baseline MPPI controllers W/WO VDG, PRED-MPPI yields improvements of 23.4% and 22.9% in RMSE, along with 36.8% and 51.6% reductions in tracking error standard deviation.

These comparative quantitative results clearly demonstrate the superior performance of the proposed PRED-MPPI in terms of computation and tracking performance.

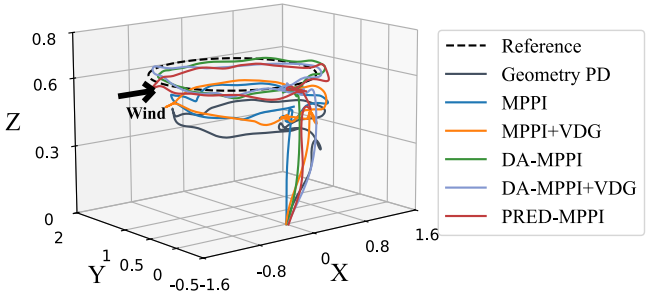

Fig. 9: Comparative circular trajectory tracking results of 6 controllers under fan-induced unknown time-varying wind.

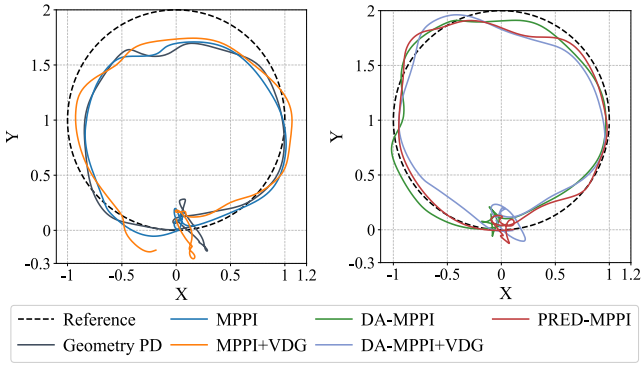

Fig. 10: Comparative circular trajectory tracking results in X-Y plane under fan-induced time-varying wind disturbances.

VI. Conclusions

This paper introduces PRED-MPPI, the first disturbance-aware and computationally efficient MPPI that integrates a Generalized Extended State Observer for disturbance preview and a Variable Discretization Grid strategy for efficient trajectory rollouts. By jointly leveraging disturbance preview and adaptive discretization, PRED-MPPI effectively handles *time-varying and mismatched disturbances* while reducing computational burden and control variance. Extensive comparative AirSim simulation and real-world quadrotor experiments validate the approach, demonstrating consistent improvements in robustness, accuracy, and efficiency over baseline MPPI, DA-MPPI, and their VDG-enhanced variants. These results establish PRED-MPPI as a disturbance-preview MPPI scheme that achieves reliable real-world quadrotor control at real-time rates. Future research will pursue the following directions progressively:

(i) rigorous **theoretical analysis** of stability and convergence under variable discretization;
(ii) fully **onboard deployment** on resource-constrained UAVs to demonstrate practical autonomy:
(iii) integration with generative samplers, such as diffusion-based models, to further improve **sample efficiency**;
(iv) **broader deployment** across heterogeneous robotic platforms, moving toward scalable and safety-critical applications in real-world environments.

References

[1] G. Williams, A. Aldrich, and E. A. Theodorou, "Model predictive path integral control: From theory to parallel computation," *Journal of Guidance, Control, and Dynamics*, vol. 40, no. 2, pp. 344–357, 2017.

[2] B. Vlahov, J. Gibson, M. Gandhi, and E. A. Theodorou, "Mppi-generic: A cuda library for stochastic optimization," *arXiv preprint arXiv:2409.07563*, 2024.

[3] W. Li, J. Su, C. Liu, W.-H. Chen, and S. Li, "Dr-mpc: Disturbance-resilient model predictive visual servoing control for quadrotor uav pipeline inspection," in *2025 IEEE/RSJ International Conference on Intelligent Robots and Systems (IROS)*. IEEE, 2025, pp. 20 738–20 745.

[4] J. Pravitra, K. A. Ackerman, C. Cao, N. Hovakimyan, and E. A. Theodorou, "L1-adaptive mppi architecture for robust and agile control of multirotors," in *2020 IEEE/RSJ International Conference on Intelligent Robots and Systems (IROS)*. IEEE, 2020, pp. 7661–7666.

[5] H. Zhang, J. Su, J. Yang, and S. Li, "Da-mppi: Disturbance-aware model predictive path integral via active disturbance estimation and compensation," in *2025 IEEE/RSJ International Conference on Intelligent Robots and Systems (IROS)*. IEEE, 2025, pp. 3752–3759.

[6] W.-H. Chen, J. Yang, L. Guo, and S. Li, "Disturbance-observer-based control and related methods—an overview," *IEEE Transactions on industrial electronics*, vol. 63, no. 2, pp. 1083–1095, 2015.

[7] F. Zhang and L. Wang, "Disturbance rejection design for gaussian process-based model predictive control using extended state observer," *Computers & Chemical Engineering*, vol. 186, p. 108708, 2024.

[8] M. O'Connell, G. Shi, X. Shi, K. Azizzadenesheli, A. Anandkumar, Y. Yue, and S.-J. Chung, "Neural-fly enables rapid learning for agile flight in strong winds," *Science Robotics*, vol. 7, no. 66, p. eabm6597, 2022.

[9] J. Chen, Y. Xu, J. Su, K. Gu, F. Wang, and S. Li, "Pet-node: Embedding priors and time-series features into neural ode," in *2025 IEEE/RSJ International Conference on Intelligent Robots and Systems (IROS)*. IEEE, 2025, pp. 18 474–18 481.

[10] J. Su, X. Zhu, S. Li, and W.-H. Chen, "Ai meets uavs: A survey on ai empowered uav perception systems for precision agriculture," *Neurocomputing*, vol. 518, pp. 242–270, 2023.

[11] J. Yang, W. X. Zheng, S. Li, B. Wu, and M. Cheng, "Design of a prediction-accuracy-enhanced continuous-time mpc for disturbed systems via a disturbance observer," *IEEE Transactions on Industrial Electronics*, vol. 62, no. 9, pp. 5807–5816, 2015.

[12] S. Zhan, W.-H. Chen, T. Steffen, and J. V. Ringwood, "Computationally efficient infinite-horizon indefinite model predictive control with disturbance preview information," *Automatica*, vol. 146, p. 110667, 2022.

[13] J. Su, W.-H. Chen, and J. Yang, "On relationship between time-domain and frequency-domain disturbance observers and its applications," *Journal of Dynamic Systems, Measurement, and Control*, vol. 138, no. 9, p. 091013, 2016.

[14] S. Zhan, Y. Chen, and J. V. Ringwood, "Computationally-efficient nonlinear model predictive control of wave energy converters with imperfect wave excitation previews," *Ocean Engineering*, vol. 319, p. 120125, 2025.

[15] G. Williams, P. Drews, B. Goldfain, J. M. Rehg, and E. A. Theodorou, "Information-theoretic model predictive control: Theory and applications to autonomous driving," *IEEE Transactions on Robotics*, vol. 34, no. 6, pp. 1603–1622, 2018.

[16] J. Alvarez-Padilla, J. Z. Zhang, S. Kwok, J. M. Dolan, and Z. Manchester, "Real-time whole-body control of legged robots with model-predictive path integral control," in *2025 IEEE International Conference on Robotics and Automation (ICRA)*. IEEE, 2025, pp. 14 721–14 727.

[17] T. Power and D. Berenson, "Learning a generalizable trajectory sampling distribution for model predictive control," *IEEE Transactions on Robotics*, vol. 40, pp. 2111–2127, 2024.

[18] G. Williams, A. Aldrich, and E. Theodorou, "Model predictive path integral control using covariance variable importance sampling," *arXiv preprint arXiv:1509.01149*, 2015.

[19] T. Han, A. Liu, A. Li, A. Spitzer, G. Shi, and B. Boots, "Model predictive control for aggressive driving over uneven terrain," *arXiv preprint arXiv:2311.12284*, 2023.

[20] W. Xiao, H. Xue, T. Tao, D. Kalaria, J. M. Dolan, and G. Shi, "Anycar to anywhere: Learning universal dynamics model for agile and adaptive mobility," in *2025 IEEE International Conference on Robotics and Automation (ICRA)*. IEEE, 2025, pp. 8819–8825.

[21] H. Xue, C. Pan, Z. Yi, G. Qu, and G. Shi, "Full-order sampling-based mpc for torque-level locomotion control via diffusion-style annealing," in *2025 IEEE International Conference on Robotics and Automation (ICRA)*. IEEE, 2025, pp. 4974–4981.

[22] Z. Yi, C. Pan, G. He, G. Qu, and G. Shi, "Covo-mpc: Theoretical analysis of sampling-based mpc and optimal covariance design," in *6th Annual Learning for Dynamics & Control Conference*. PMLR, 2024, pp. 1122–1135.

[23] C. Liu, W.-H. Chen, and J. Andrews, "Tracking control of small-scale helicopters using explicit nonlinear mpc augmented with disturbance observers," *Control Engineering Practice*, vol. 20, no. 3, pp. 258–268, 2012.

[24] M. S. Gandhi, B. Vlahov, J. Gibson, G. Williams, and E. A. Theodorou, "Robust model predictive path integral control: Analysis and performance guarantees," *IEEE Robotics and Automation Letters*, vol. 6, no. 2, pp. 1423–1430, 2021.

[25] X. Zhang, J. Lu, Y. Hui, H. Shen, L. Xu, and B. Tian, "Rapa-planner: Robust and efficient motion planning for quadrotors based on parallel ra-mppi," *IEEE Transactions on Industrial Electronics*, vol. 72, no. 7, pp. 7149–7159, 2025.

[26] T. Li, Z. Zhao, S. Ding, and J. Su, "Composite controller design for quadrotor uavs with uncertainties and noises based on combined kalman filter and gpio," *IEEE Transactions on Aerospace and Electronic Systems*, vol. 60, no. 1, pp. 882–892, 2023.

[27] T. Lee, M. Leok, and N. H. McClamroch, "Geometric tracking control of a quadrotor uav on se (3)," in *49th IEEE conference on decision and control (CDC)*. IEEE, 2010, pp. 5420–5425.

[28] Z. Feng, L. Qiu, and S. Bansal, "Bridging model predictive control and deep learning for scalable reachability analysis," *arXiv preprint arXiv:2505.03830*, 2025.

[29] S. Li, J. Yang, W.-H. Chen, and X. Chen, "Generalized extended state observer based control for systems with mismatched uncertainties," *IEEE Transactions on Industrial Electronics*, vol. 59, no. 12, pp. 4792–4802, 2011.

[30] J. Yin, O. So, E. Y. Yu, C. Fan, and P. Tsiotras, "Safe beyond the horizon: Efficient sampling-based mpc with neural control barrier functions," *arXiv preprint arXiv:2502.15006*, 2025.